

Collect-and-Distribute Transformer for 3D Point Cloud Analysis

Haibo Qiu · Baosheng Yu · Dacheng Tao

Received: date / Accepted: date

Abstract Remarkable advancements have been made recently in point cloud analysis through the exploration of transformer architecture, but it remains challenging to effectively learn local and global structures within point clouds. In this paper, we propose a new transformer network equipped with a collect-and-distribute mechanism to communicate short- and long-range contexts of point clouds, which we refer to as CDFormer. Specifically, we first employ self-attention to capture short-range interactions within each local patch, and the updated local features are then collected into a set of proxy reference points from which we can extract long-range contexts. Afterward, we distribute the learned long-range contexts back to local points via cross-attention. To address the position clues for short- and long-range contexts, we additionally introduce the context-aware position encoding to facilitate position-aware communications between points. We perform experiments on five popular point cloud datasets, namely ModelNet40, ScanObjectNN, ShapeNetPart, S3DIS and ScanNetV2, for classification and segmentation. Results show the effectiveness of the proposed CDFormer, delivering several new state-of-the-art performances on point cloud classification and segmentation tasks. The source code is available at <https://github.com/haibo-qiu/CDFormer>.

Keywords Point Cloud Analysis, Transformer, Collect-Distribute, Segmentation, Classification

Haibo Qiu · Baosheng Yu · Dacheng Tao
{hqiu2518, baosheng.yu, dacheng.tao}@sydney.edu.au

School of Computer Science, the University of Sydney,
Sydney NSW, 2008, Australia

1 Introduction

Point clouds have been extensively investigated in recent years, mainly due to their numerous promising real-world applications, such as autonomous driving (Aksoy et al., 2020; Li et al., 2020) and robotics (Li et al., 2019; Yang et al., 2020). Unlike 2D images, a point cloud is a set of 3D points distributed in an irregular and disordered manner, where each point is usually characterized by its Cartesian coordinates (x, y, z) . These fundamental differences make it non-trivial to utilize off-the-shelf 2D deep architectures for point cloud analysis. Therefore, many recent methods have developed different deep architectures to handle the special characteristics of point clouds, including mlp-based (Ma et al., 2022; Qi et al., 2017a,b), cnn-based (Li et al., 2018b), and graph-based models (Thomas et al., 2019; Wang et al., 2019). These architectures aim to address the challenges posed by the irregularity and unordered nature of point clouds and enable effective point cloud analysis.

One of the main challenges in point cloud analysis is efficiently exploring local and global features while considering the irregular and disordered characteristics of point clouds. Recently, transformer architectures, which enable effective local/global-range learning via the attention mechanism, have become popular in both natural language processing (Brown et al., 2020; Devlin et al., 2018; Vaswani et al., 2017) and computer vision (Dosovitskiy et al., 2020; Liu et al., 2021a; Wang et al., 2021, 2022). Inspired by this, transformer architectures have been further introduced for point cloud analysis (Guo et al., 2021; Lai et al., 2022; Park et al., 2022; Zhao et al., 2021). However, the vanilla self-attention module in transformer has a time complexity of $\mathcal{O}(N^2)$ when operating on a sequence of tokens

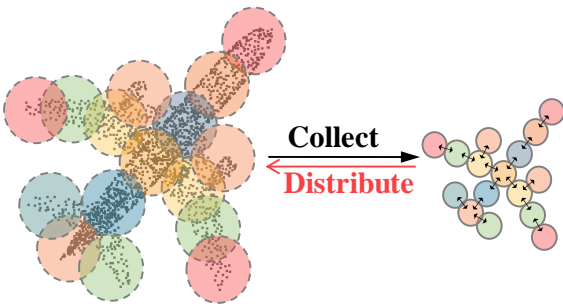


Fig. 1: An illustration of the proposed collect-and-distribute mechanism.

with length N . When taking each point as a token, the $\mathcal{O}(N^2)$ complexity becomes unaffordable, as there are tens of thousands of points for each point cloud in real-world applications (Armeni et al., 2016). To address this challenge, Zhao et al. (2021) introduces vector self-attention in a local way, avoiding $\mathcal{O}(N^2)$ complexity by only interacting features with K neighbors (e.g., $K = 16$), while failing to capture long-range contexts. On the other hand, Lai et al. (2022) employs local window-based self-attention with a shifted window strategy similar to Liu et al. (2021a) and proposes to capture long-range contexts by sampling nearby points densely and distant points sparsely. Nevertheless, due to the heterogeneous density distribution of point clouds, the fixed-size window partition employed in Lai et al. (2022) leads to a diverse number of points in each local window, thus requiring complicated and sophisticated designs during implementation.

In this work, we propose a new collect-and-distribute transformer, CDFormer, to learn both short- and long-range contexts for 3D point cloud analysis. Specifically, we first divide the point cloud into a set of local patches using K nearest neighbor points, instead of a fixed window partition (Lai et al., 2022). Each local patch contains the same number of points, enabling direct modeling by popular deep learning packages (Abadi et al., 2016; Paszke et al., 2019) without custom operations and avoids the prohibitive $\mathcal{O}(N^2)$ time complexity. Besides local self-attention for short-range interactions within each local patch, we introduce a collect-and-distribute mechanism. This mechanism first collects local patch information to a set of proxy reference points, explores long-range contexts among these reference points, and distributes the collected long-range contexts back to local points through cross-attention between reference points and local points. An illustration of the proposed collect-and-distribute mechanism is shown in Figure 1. To enhance local-global structure learning, the positional information is critical for transformers employed in point clouds (Lai et al., 2022; Zhao

et al., 2021). Therefore, we introduce context-aware position encoding for CDFormer, where the relative position information interacts with the input features to dynamically enhance the positional clues.

Our main contributions can be summarized as follows:

- We propose CDFormer to capture short- and long-range contexts simultaneously with a novel collect-and-distribute mechanism, effectively learning local-global structures.
- We introduce context-aware position encoding to enhance position clues and facilitate communications within points.
- We perform extensive experiments on five well-known point cloud datasets: ModelNet40 (Wu et al., 2015) and ScanObjectNN (Uy et al., 2019) for classification, along with ShapeNetPart (Yi et al., 2016), S3DIS (Armeni et al., 2016), and ScanNetV2 (Dai et al., 2017) for segmentation. The experimental results and analysis demonstrate the effectiveness of CDFormer and achieve state-of-the-art performances in point cloud processing.

2 Related Work

Transformer Architectures. Transformer architectures have emerged as a dominant framework for natural language processing in recent years (Devlin et al., 2018; Vaswani et al., 2017). In addition, they have seen widespread exploration in the realm of vision tasks, with ViT (Dosovitskiy et al., 2020) being a groundbreaking work that divides images into local patches and treats each patch as a token. Building upon the success of ViT, numerous subsequent works have been proposed that either explore hierarchical architectures with multi-scale resolutions (Fan et al., 2021a; Gu et al., 2022; Li et al., 2022b; Liu et al., 2021a; Wang et al., 2021, 2022) or incorporate local-global information (Chu et al., 2021; Li et al., 2022a; Yang et al., 2021). For instance, PVT (Wang et al., 2021) devises a progressive shrinking pyramid to effectively explore multi-resolution features while HRViT (Gu et al., 2022) integrates high-resolution multi-branch architectures to learn multiplicative scale representations. Twins-SVT (Chu et al., 2021) incorporates locally-grouped self-attention and global sub-sampled attention to capture local-global contexts. Swin Transformer (Liu et al., 2021a) introduces a hierarchical transformer architecture equipped with the shifted window strategy to enable cross-window communications. SepViT (Li et al., 2022a) proposes a self-attention mechanism that is depthwise separable to facilitate efficient local and global information exchange within a single attention block.

Point Cloud Analysis. The mainstream point cloud analysis methods can be roughly divided into three directories: point-based (Guo et al., 2021; Lai et al., 2022; Li et al., 2018b; Ma et al., 2022; Park et al., 2022; Qian et al., 2022; Qi et al., 2017a,b; Qiu et al., 2023; Tang et al., 2023; Thomas et al., 2019; Wang et al., 2019; Xu et al., 2021a; Zhao et al., 2021), voxel-based (Cheng et al., 2021a; Tang et al., 2020; Zhu et al., 2021), and projection-based (Cortinhal et al., 2020; Qiu et al., 2022; Milioto et al., 2019; Zhang et al., 2020). For a better trade-off between complexity and efficiency, we focus primarily on point-based approaches, where existing methods usually devise novel operations/architectures for raw points, including mlp-based (Ma et al., 2022; Qian et al., 2022; Qi et al., 2017a,b), cnn-based (Li et al., 2018b), graph-based (Thomas et al., 2019; Wang et al., 2019), and transformer-based (Guo et al., 2021; Lai et al., 2022; Park et al., 2022; Zhao et al., 2021). A pioneering work in this field is PointNet (Qi et al., 2017a), which directly processes point clouds using multi-layer perceptrons (MLPs). This approach was further improved upon by PointNet++ (Qi et al., 2017b), which introduced a hierarchical structure for processing point clouds. PointNext (Qian et al., 2022) proposes even more improved training strategies that significantly improve upon PointNet++ (Qi et al., 2017b). PointCNN (Li et al., 2018b) learns an x-transformation from the input points for alignment, which is followed by typical convolution layers. In contrast, KPConv (Thomas et al., 2019) introduces kernel point convolution, a new point convolution operator, that takes neighboring points as input and processes them with spatially located weights. Recently, transformer architectures have been introduced for point cloud analysis (Guo et al., 2021; Lai et al., 2022; Park et al., 2022; Zhao et al., 2021). PCT (Guo et al., 2021) presents the offset-attention mechanism, which replaces the original self-attention. Point Transformer (Zhao et al., 2021) proposes to introduce a vector self-attention mechanism to aggregate neighbor features but fails to capture long-range dependencies. Stratified Transformer (Lai et al., 2022) captures long-range contexts by sampling nearby points densely and distant points sparsely with the shifted window strategy, as used in Swin Transformer (Liu et al., 2021a). However, due to the varying density distribution of point clouds, partitioning windows in a fixed size leads to varying point counts in different local windows, requiring sophisticated designs to address this issue.

3 Method

In this section, we first provide an overview of the proposed CDFormer for 3D point cloud analysis. We then

introduce the patch division and the collect-and-distribute mechanism in detail. Lastly, we discuss the proposed context-aware position encoding.

3.1 Overview

A 3D point cloud usually consists of a set of N points $\mathbf{P} \in \mathbb{R}^{N \times 3}$, where each point is featured by the Cartesian coordinate (x, y, z) . The objective of typical point cloud analysis tasks is to assign semantic labels to the point cloud. For example, for point cloud classification, the goal is to predict a single semantic label $Q \in \{0, \dots, U-1\}$ for the whole point cloud \mathbf{P} , where U is the total number of semantic categories. For point cloud segmentation, the goal is to assign a semantic label for each point in the point cloud \mathbf{P} .

The main CDFormer framework for 3D point cloud analysis is illustrated by Figure 2. Since a point cloud may also contain extra features such as color, we consider the input feature of a general point cloud as $\mathbf{X} \in \mathbb{R}^{N \times C}$, where C indicates the number of feature channels. Specifically, we first utilize a KPConv (Thomas et al., 2019) layer as the embedding layer to aggregate local information for raw point embeddings to obtain the embedded features with the size of $N \times C_1$. After that, the main backbone network is a stack of multiple the proposed collect-and-distribute blocks or CD Blocks, where each block first divides all points into local patches and then explores short- and long-range contexts in a collect-and-distribute manner as follows: 1) a local self-attention is first used to learn short-range relations in each patch of points; 2) the learned local features are then collected to a set of proxy reference points which then communicate with each other to capture long-range contexts; and 3) the learned long-range contexts are finally distributed back to the original local patch points such that the learned point embeddings are equipped with both short- and long-range information. CDFormer is built by stacking multiple downsampling layers and CD Blocks.

3.2 Patch Division

For a typical point cloud with tens of thousands of points (Armeni et al., 2016), it is computationally prohibitive to consider each point as a token: given a sequence of tokens with the length N , the time complexity of the self-attention in transformer is $\mathcal{O}(N^2)$. Therefore, following (Dosovitskiy et al., 2020; Pang et al., 2022; Yu et al., 2022), we divide a point cloud into multiple local patches, *e.g.*, M patches with K points in each patch, and then employ self-attention within each local patch

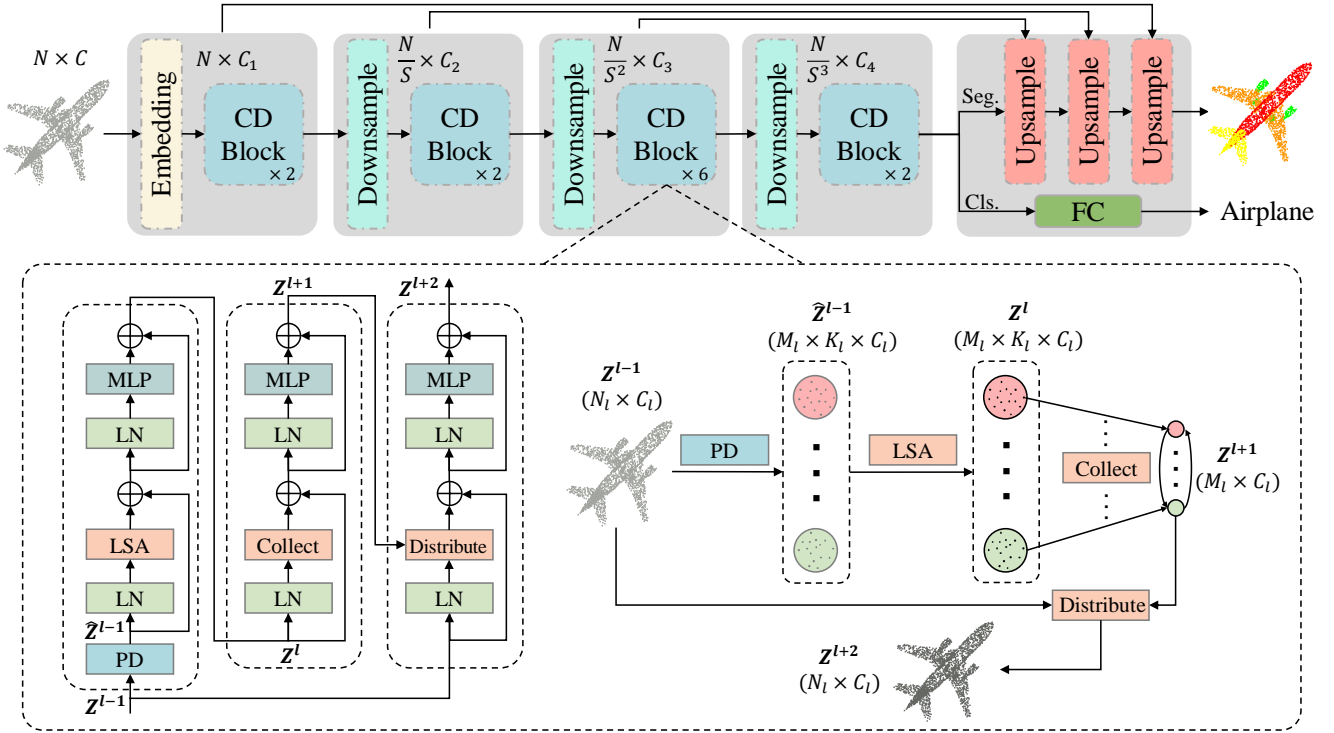


Fig. 2: The main collect-and-distribute transformer framework. Note that **PD** refers to patch division and **LSA** indicates the local self-attention defined by Equation 1 and 2.

instead of all points. Therefore, with a proper patch division, it becomes acceptable with a linear time complexity $\mathcal{O}(MK^2)$.

We describe the patch division process used in our method as follows. Given a scale factor S , the furthest point sampling algorithm (FPS) (Eldar et al., 1997; Qi et al., 2017b) is applied on the point features $\mathbf{X} \in \mathbb{R}^{N \times C}$ to obtain patch centers $\hat{\mathbf{X}} \in \mathbb{R}^{M \times C}$ where $M = N/S$. For each local patch, we group the K nearest neighbors around each patch center and reformulate M patches as $\hat{\mathbf{X}} \in \mathbb{R}^{M \times K \times C}$, and then apply the local self-attention (LSA) to extract local features. Specifically, for the i_{th} patch where $i \in [0, \dots, M-1]$, let $\hat{\mathbf{x}} \in \mathbb{R}^{K \times C}$ denote its representation, which is then fed into MLPs to generate the query token $\mathbf{Q}_{lsa} = \mathbf{W}_{lsa}^q \hat{\mathbf{x}}$, the key token $\mathbf{K}_{lsa} = \mathbf{W}_{lsa}^k \hat{\mathbf{x}}$, and the value token $\mathbf{V}_{lsa} = \mathbf{W}_{lsa}^v \hat{\mathbf{x}}$, respectively. The output $\bar{\mathbf{z}} \in \mathbb{R}^{K \times C}$ can thus be calculated as follows:

$$\bar{\mathbf{z}} = \mathbf{W}_{lsa}^{attn} \mathbf{V}_{lsa}, \quad (1)$$

$$\mathbf{W}_{lsa}^{attn} = \text{Softmax}((\mathbf{Q}_{lsa} \mathbf{K}_{lsa}^T) / \sqrt{C}). \quad (2)$$

All M patches features can be similarly obtained as $\bar{\mathbf{Z}} \in \mathbb{R}^{M \times K \times C}$. Notably, we do not discuss the position encoding here and leave it in Sec 3.4. Lastly, we have the complexity as follows: the local self-attention in each patch only has the time complexity $\mathcal{O}(K^2)$, and the

overall time complexity of M patches become affordable $\mathcal{O}(MK^2) = \mathcal{O}(NK^2/S)$. Through LSA, all points in each local patch can communicate with each other to capture short-range dependencies.

3.3 Collect-and-Distribute Mechanism

As the aforementioned local self attention only models the short-range information in each local patch, we then introduce how to explore long-range contexts with the proposed collect-and-distribute mechanism. Specifically, we first collect those communicated local feature as a set of proxy reference points such that each local patch directly corresponds to a specific proxy point. To capture the long-range dependencies, a neighbor self-attention (NSA) is then applied on those proxy references to allow feature propagation among neighbors. By doing this, we can extract long-range contexts with a reduced linear time complexity since each proxy represents a patch of points. Lastly, those enhanced proxies distribute back to the local points via cross-attention to achieve short- and long-range contexts communications. An illustration of the proposed block is shown in Figure 3, and we depict each step in detail as follows.

Collect. Given local patches $\bar{\mathbf{Z}} \in \mathbb{R}^{M \times K \times C}$, we collect local patch information from all K local points to

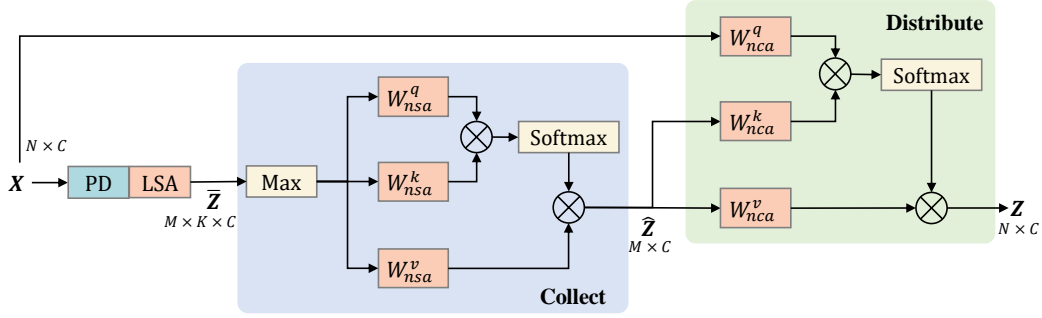


Fig. 3: Collect-and-distribute block. Note that **Collect** involves the neighbor self-attention (nsa) defined by Equation 3 and 4; **Distribute** includes the neighbor cross-attention (nca) formulated in Equation 5 and 6.

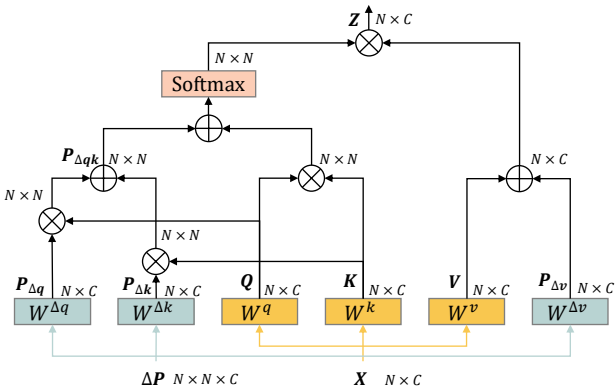


Fig. 4: Context-aware position encoding.

a proxy reference point via a max-pooling operation, $\mathbf{R} = \text{maxpool}(\bar{\mathbf{Z}}) \in \mathbb{R}^{M \times C}$. Next, we consider the K nearest neighbors for each proxy $\hat{\mathbf{R}} \in \mathbb{R}^{M \times K \times C}$ to capture the long-range contexts by employing a neighboring self-attention between \mathbf{R} and $\hat{\mathbf{R}}$, *i.e.*, a self-attention between each proxy and its K neighbors followed by a sum operation to generate the output $\hat{\mathbf{Z}} \in \mathbb{R}^{M \times C}$. We first generate the feature embeddings with MLPs for query, key, and value by $\mathbf{Q}_{nsa} = \mathbf{W}_{nsa}^q \mathbf{R}$, $\mathbf{K}_{nsa} = \mathbf{W}_{nsa}^k \hat{\mathbf{R}}$, and $\mathbf{V}_{nsa} = \mathbf{W}_{nsa}^v \hat{\mathbf{R}}$, respectively. Then we can formulate the process as follows:

$$\hat{\mathbf{Z}} = \text{Sum}(\mathbf{W}_{nsa}^{attn} \mathbf{V}_{nsa}) \quad (3)$$

$$\mathbf{W}_{nsa}^{attn} = \text{Softmax}((\mathbf{Q}_{nsa} \mathbf{K}_{nsa}^T) / \sqrt{C}). \quad (4)$$

Notably, the time complexity $\mathcal{O}(NK^2/S)$ is linear to N because the NSA is only applied on K neighbors instead of all proxies.

Distribute. We distribute the long-range information in $\hat{\mathbf{Z}} \in \mathbb{R}^{M \times C}$ back to local patch points for joint short- and long-range contexts via a neighbor cross-attention (NCA). In particular, given vanilla point features $\mathbf{X} \in \mathbb{R}^{N \times C}$ and enhanced proxies $\hat{\mathbf{Z}} \in \mathbb{R}^{M \times C}$, we first group the K nearest neighbor proxies $\mathbf{E} \in$

$\mathbb{R}^{N \times K \times C}$ for each point. After that, we employ the neighbor cross-attention by regarding \mathbf{X} as the query, \mathbf{E} as the key and value, which is fed into a successive sum operation to obtain the final output $\mathbf{Z} \in \mathbb{R}^{N \times C}$. We first get the embeddings with MLPs by $\mathbf{Q}_{nca} = \mathbf{W}_{nca}^q \mathbf{X}$, $\mathbf{K}_{nca} = \mathbf{W}_{nca}^k \mathbf{E}$, and $\mathbf{V}_{nca} = \mathbf{W}_{nca}^v \mathbf{E}$, respectively. After that, we can calculate \mathbf{Z} as follows:

$$\mathbf{Z} = \text{Sum}(\mathbf{W}_{nca}^{attn} \mathbf{V}_{nca}) \quad (5)$$

$$\mathbf{W}_{nca}^{attn} = \text{Softmax}((\mathbf{Q}_{nca} \mathbf{K}_{nca}^T) / \sqrt{C}). \quad (6)$$

In this way, each point communicates with K enhanced proxies, *i.e.*, approximate K^2 original proxies, and K^3 original points. Therefore, the long-range dependencies can be effectively distributed back to local points, *i.e.*, both short- and long-range contexts are fused into the learned representations.

3.4 Context-Aware Position Encoding

The position information of input tokens is necessary for transformer architectures (Dosovitskiy et al., 2020; Vaswani et al., 2017), while 3D point cloud naturally contains the (x, y, z) coordinates as position. Therefore, it might be straightforward to remove position encoding in the transformer-based architecture for point clouds. However, when the network goes deeper, the coordinates information can not keep precisely intact (Lai et al., 2022; Zhao et al., 2021). Inspired by Wu et al. (2021), we propose to further enhance the position clues in point cloud transformer via a context-aware position encoding (CAPE). Specifically, CAPE is calculated by interacting relative position differences with the current features, thus can simultaneously handle the unordered characteristic of the point cloud and adaptively enhance the position information. An illustration of the proposed context-aware position encoding is shown in Figure 4.

Given the input $\mathbf{X} \in \mathbb{R}^{N \times C}$ and the relative position differences $\Delta \mathbf{P} \in \mathbb{R}^{N \times N \times 3}$, we first obtain the $\mathbf{Q}, \mathbf{K}, \mathbf{V}$ and their position embeddings $\mathbf{P}_{\Delta q}, \mathbf{P}_{\Delta k}, \mathbf{P}_{\Delta v}$ via MLPs. We then calculate the CAPE by:

$$\mathbf{P}_{\Delta qk} = \mathbf{P}_{\Delta q} \mathbf{Q}^\top + \mathbf{P}_{\Delta k} \mathbf{K}^\top, \quad (7)$$

such that it is aware of the input features and can dynamically magnify the position information to effectively facilitate the communication of points. Lastly, we obtain the output $\mathbf{Z} \in \mathbb{R}^{N \times C}$ as follows:

$$\mathbf{Z} = \mathbf{W}_{attn} \cdot (\mathbf{V} + \mathbf{P}_{\Delta v}) \quad (8)$$

$$\mathbf{W}_{attn} = \text{Softmax}((\mathbf{Q} \mathbf{K}^\top + \mathbf{P}_{\Delta qk}) / \sqrt{C}). \quad (9)$$

Notably, if not otherwise stated, we use CAPE in all attention layers, including LSA, NSA, and NCA, to better capture short- and long-range contexts.

4 Experiments

In this section, we first introduce the implementation details. We then evaluate the proposed CDFormer on ModelNet40 (Wu et al., 2015) and ScanObjectNN (Uy et al., 2019) for point cloud classification, ShapeNetPart (Yi et al., 2016) for point cloud part segmentation, as well as S3DIS (Armeni et al., 2016) and ScanNetV2 (Dai et al., 2017) for point cloud scene segmentation. Lastly, we perform comprehensive ablation studies on each component.

4.1 Implementation Details.

For ModelNet40 (Wu et al., 2015), following Qian et al. (2022), we use fewer blocks in each stage [1, 1, 3, 1] with larger feature dimensions $\mathcal{C} = [64, 128, 256, 512]$ and larger number of heads $\mathcal{H} = [4, 8, 16, 32]$. We simply use $K = 16$ neighbours in all blocks. Cosine annealing schedule with learning rate 0.001 is adopted for training 600 epochs with batch size 32. We use AdamW optimizer (Loshchilov and Hutter, 2017) with the weight decay 0.05. For each data sample, only 1,024 points with (x, y, z) are used for training and testing, and common data augmentations, including shift, scale and cutmix (Zhang et al., 2022), are employed. The downsampling scale S of each stage is set to 4. For ScanObjectNN (Uy et al., 2019), we follow Qian et al. (2022) to use point resampling to adapt 1,024 points for training, and only the hardest perturbed variant (PB.T50_RS) is considered in our experiment. We keep other training configurations the same as those in ModelNet40.

For S3DIS (Armeni et al., 2016), following the practice in Lai et al. (2022); Zhao et al. (2021), we first

apply the grid sampling on the raw input points with the grid size 0.04m. We adopt the encoder with four stages with [2, 2, 6, 2] blocks, the number of channels $\mathcal{C} = [C_1, C_2, C_3, C_4] = [48, 96, 192, 384]$ and the number of heads $\mathcal{H} = [H_1, H_2, H_3, H_4] = [3, 6, 12, 24]$. For simplicity, we set neighbours $K = 16$ in all blocks. During the training process, the maximum number of input points is set to 80,000. Meanwhile, we set the downsampling scale S of each stage to 8. We use AdamW optimizer (Loshchilov and Hutter, 2017) with the weight decay 0.01. All models are trained for 100 epochs, and the learning rate starts from 0.01 and drops by 1/10 at 60 and 80 epochs. We use four V100 GPUs with the batch size of 8. Following Qian et al. (2022), we use the cross-entropy loss with label smoothing, and popular data augmentations including jitter, scale, rotate, and color drop. For ScanNetV2 (Dai et al., 2017), we use grid sampling with a size of 0.02m on the raw point clouds, following Wu et al. (2022). We employ the OneCycleLR (Smith and Topin, 2019) scheduler, which increases the learning rate from 0.0005 to 0.005 in the first 5 epochs and then uses cosine annealing to decrease it to 0 over the remaining 95 epochs. Additionally, we repeat the training set (1,201 scenes) 9 times to obtain 10,809 samples during the training process. For ShapeNetPart (Yi et al., 2016), we follow Qian et al. (2022) to use 2,048 points for training and testing. Considering that each point cloud has fewer points than it in S3DIS (Armeni et al., 2016), we reduce the downsampling scale S to 4 and use the batch size 80. The model is trained for 300 epochs, and the learning rate starts from 0.01 and drops by 1/10 at 210 and 270 epochs. Other settings are same as those in S3DIS.

4.2 Point Cloud Classification

Dataset and Metrics. ModelNet40 (Wu et al., 2015) is a canonical dataset for object shape classification, which consists of 9,843 training and 2,468 testing CAD models belonging to 40 categories. We report the results of overall accuracy (OA). ScanObjectNN (Uy et al., 2019) is a more challenging real-world benchmark in terms of background, noise, and occlusions. It contains totally 15,000 objects from 15 classes. We report the results of the mean of class-wise accuracy (mAcc) and overall accuracy (OA) on hardest perturbed variant, *i.e.*, PB.T50_RS.

Results. Table 1 shows the results on ModelNet40, where the proposed CDFormer achieves comparable performance 94.0% with other state-of-the-arts by only taking 1,024 points as input. In Table 2, we also evaluate the proposed method on the most challenging vari-

Table 1: Results on ModelNet40.

Method	#Points	OA (%)
PointNet (Qi et al., 2017a)	1024	89.2
PointNet++ (Qi et al., 2017b)	1024	90.7
PointNet++ (Qi et al., 2017b)	5000	91.9
PointCNN (Li et al., 2018b)	1024	92.5
PointConv (Wu et al., 2019)	1024	92.5
A-CNN (Komarichev et al., 2019)	1024	92.6
KPConv (Thomas et al., 2019)	7000	92.9
DGCNN (Wang et al., 2019)	1024	92.9
PointASNL (Yan et al., 2020)	1024	92.9
PointNext (Qian et al., 2022)	1024	93.2
PosPool (Liu et al., 2020)	5000	93.2
PCT (Guo et al., 2021)	1024	93.2
SO-Net (Li et al., 2018a)	5000	93.4
PT (Zhao et al., 2021)	1024	93.7
GBNet (Qiu et al., 2021b)	1024	93.8
PA-DGC (Xu et al., 2021b)	1024	93.9
PointMLP (Ma et al., 2022)	1024	94.1
CDFormer (ours)	1024	<u>94.0</u>

Table 2: Results on ScanObjectNN.

Method	mAcc (%)	OA (%)
PointNet (Qi et al., 2017a)	63.4	68.2
SpiderCNN (Xu et al., 2018)	69.8	73.7
PointNet++ (Qi et al., 2017b)	75.4	77.9
DGCNN (Wang et al., 2019)	73.6	78.1
PointCNN (Li et al., 2018b)	75.1	78.5
BGA-DGCNN (Uy et al., 2019)	75.7	79.7
BGA-PN++ (Uy et al., 2019)	77.5	80.2
DRNet (Qiu et al., 2021a)	78.0	80.3
GBNet (Qiu et al., 2021b)	77.8	80.5
SimpleView (Goyal et al., 2021)	-	80.5±0.3
PRANet (Cheng et al., 2021b)	79.1	82.1
MVTN (Hamdi et al., 2021)	-	82.8
PointMLP (Ma et al., 2022)	83.9±0.5	85.4±0.3
PointNext (Qian et al., 2022)	85.8±0.6	87.7±0.4
CDFormer (ours)	87.2±0.3	88.4±0.2

ant (PB_T50_RS) of ScanObjectNN, where CDFormer achieves 87.2 ± 0.3 and 88.4 ± 0.2 on mAcc and OA, outperforming all previous methods in terms of both performance and stability. Specifically, PointMLP (Ma et al., 2022) obtains 94.1% on ModelNet40, but we surpass it by over 3% in ScanObjectNN and also show more stable performance as indicated by the smaller standard deviation. PointNeXt (Qian et al., 2022) is the current state-of-the-art method, but we still outperform it by a clear margin, especially on mAcc (87.2% vs. 85.8%). Also, the smallest gap between mean of class-wise accuracy (mAcc) and overall accuracy (OA) achieved by CDFormer implies that our approach shows excellent robust performance on each class instead of biasing to a specific category. We owe it to the proposed collect-and-distribute mechanism for effectively capturing both

Table 3: Results on ShapeNetPart.

Method	mIoU (%)	Speed
PointNet (Qi et al., 2017a)	83.7	1184
PointNet++ (Qi et al., 2017b)	85.1	<u>708</u>
DGCNN (Wang et al., 2019)	85.2	147
ASSANet-L (Qian et al., 2021)	86.1	640
PointMLP (Ma et al., 2022)	86.1	270
KPConv (Thomas et al., 2019)	86.4	44
PT (Zhao et al., 2021)	86.6	297
StratifiedFormer (Lai et al., 2022)	86.6	398
CurveNet (Xiang et al., 2021)	<u>86.8</u>	97
PointNeXt (Qian et al., 2022)	87.0	76
CDFormer (ours)	87.0	84

short- and long-range contexts, which can handle different categories with different scales and shapes.

4.3 Point Cloud Part Segmentation

Dataset and Metrics. ShapeNetPart (Yi et al., 2016) is a popular dataset for object part segmentation, which is composed of 16,880 3D models from 16 different shape categories (*e.g.*, “airplane” and “chair”), where 14,006 models for training and 2,874 for testing. For each category, its number of parts is between 2 and 6, and there are total 50 different parts. For evaluation metrics, we report the instance mIoU along with the throughput speed (*instance/second*).

Results. Table 3 demonstrates the results of CDFormer compared to previous approaches. Our CDFormer outperforms congeneric transformer-based methods, *e.g.*, Point Transformer (Zhao et al., 2021) and Stratified Transformer (Lai et al., 2022), and other representative approaches like KPConv (Thomas et al., 2019), while it is comparable to the best results of PointNext (Qian et al., 2022) (87.0% vs. 87.0%). As we will see from Table 4 that the CDFormer defeats PointNext on S3DIS (76.0% vs. 74.9%), we thus conjecture that the collect-and-distribute mechanism in CDFormer can not fully exploit the advantage of capturing long-range dependencies on the small size of point cloud considering the huge difference on the size of samples in ShapeNetPart (2,048) and S3DIS (up to 80,000 during training). The part segmentation results of multiple objects are visualized in Figure 5. As observed, the predictions from CDFormer are semantically reasonable and close to the ground truth, further validating its effectiveness.

4.4 Point Cloud Scene Segmentation

Dataset and Metrics. S3DIS (Armeni et al., 2016) is a widely used benchmark for point cloud scene segmen-



Fig. 5: Visualizations of object part segmentation on multiple different categories from the ShapeNetPart dataset. The top row represents ground truth and the predictions from the proposed CDFormer are in the second row.

Table 4: Results on S3DIS using 6-fold cross-validation. The **bold** and underline denote the first and second best performances. Note that * indicates additional 2D images are used and † represents the reproduced results.

Method	mIoU	mACC	OA	ceiling	floor	wall	beam	column	window	door	table	chair	sofa	bookcase	board	clutter
PointNet (Qi et al., 2017a)	47.6	66.2	78.6	88.0	88.7	69.3	42.4	23.1	47.5	51.6	54.1	42.0	9.6	38.2	29.4	35.2
RSNet (Huang et al., 2018)	56.5	66.5	-	92.5	92.8	78.6	32.8	34.4	51.6	68.1	59.7	60.1	16.4	50.2	44.9	52.0
PointCNN (Li et al., 2018b)	65.4	75.6	88.1	94.8	97.3	75.8	63.3	51.7	58.4	57.2	71.6	69.1	39.1	61.2	52.2	58.6
PointWeb (Zhao et al., 2019)	66.7	76.2	87.3	93.5	94.2	80.8	52.4	41.3	64.9	68.1	71.4	67.1	50.3	62.7	62.2	58.5
ShellNet (Zhang et al., 2019)	66.8	-	87.1	90.2	93.6	79.9	60.4	44.1	64.9	52.9	71.6	84.7	53.8	64.6	48.6	59.4
RandLA-Net (Hu et al., 2020)	70.0	82.0	88.0	93.1	96.1	80.6	62.4	48.0	64.4	69.4	69.4	76.4	60.0	64.2	65.9	60.1
KPCov (Thomas et al., 2019)	70.6	79.1	-	93.6	92.4	83.1	63.9	54.3	66.1	76.6	57.8	64.0	69.3	74.9	61.3	60.3
SCF-Net (Fan et al., 2021b)	71.6	82.7	88.4	93.3	96.4	80.9	64.9	47.4	64.5	70.1	71.4	81.6	67.2	64.4	67.5	60.9
BAAF (Qiu et al., 2021c)	72.2	<u>83.1</u>	88.9	93.3	96.8	81.6	61.9	49.5	65.4	73.3	72.0	83.7	67.5	64.3	67.0	62.4
CBL (Tang et al., 2022)	73.1	79.4	89.6	94.1	94.2	85.5	50.4	58.8	70.3	78.3	75.7	75.0	71.8	74.0	60.0	62.4
PT (Zhao et al., 2021)	73.5	81.9	90.2	-	-	-	-	-	-	-	-	-	-	-	-	-
DeepViewAgg (Robert et al., 2022)*	74.7	-	-	90.0	96.1	85.1	66.9	56.3	71.9	78.9	79.7	73.9	69.4	61.1	75.0	65.9
PointNext-XL (Qian et al., 2022)	74.9	83.0	90.3	-	-	-	-	-	-	-	-	-	-	-	-	-
PointNext-XL (Qian et al., 2022)†	<u>74.9</u>	83.0	<u>90.3</u>	94.1	96.8	85.0	61.4	64.2	68.5	78.7	76.9	70.2	74.3	70.7	69.9	63.2
CDFormer	76.0	84.6	90.7	94.4	97.8	86.7	70.8	66.7	69.1	78.9	77.8	64.9	75.3	71.4	71.1	63.6

tation, containing 271 rooms in 6 areas collected from three buildings. The point is annotated with 13 semantic categories such as “ceiling” and “bookcase”. Following Qi et al. (2017b); Zhao et al. (2021), we evaluate the proposed method on the Area 5 and also perform the standard 6-fold cross-validation. ScanNetV2 (Dai et al., 2017) is another challenging dataset that consists of 1,513 room scenes. Among these scenes, 1,201 are used for training and 312 for validation purposes. Each sampled point is assigned a semantic label from one of the available 20 categories, including “floor” and “table”. Similar to previous methods (Han et al., 2020; Liu et al., 2021b; Wu et al., 2022; Yang et al., 2023), we make evaluations on the validation and testing sets. Regarding the metrics, we report performance using mean class-wise intersection over union (mIoU), mean of class-wise accuracy (mAcc), and overall point-wise accuracy (OA) as in Qian et al. (2022); Wu et al. (2022).

Results. In Table 4 and 5, the proposed CDFormer achieves new state-of-the-art performances on both Area 5 and standard 6-fold cross-validation. Notably, the recent approach PointNext (Qian et al., 2022) has 41.6M parameters for its best results, while our CDFormer with 25.7M parameters achieves a clear improvement of 1.7% and 1.1% mIoU under Area 5 and 6-fold cross-validation. Additionally, with and without using 2D images, DeepViewAgg (Robert et al., 2022) obtains 69.5% and 74.7% respectively, which nevertheless is also inferior to CDFormer (76.0%). Additionally, we provide visualizations in Figure 6. The proposed CDFormer exhibit exceptional ability in capturing short- and long-range contexts, and accurately segmenting complicated scenes. We also present the results on ScanNetV2 in Table 6. As observed, our CDFormer achieves the best performance of 76.2% on the validation set and 76.6% on the testing set, further demonstrating its superiority.

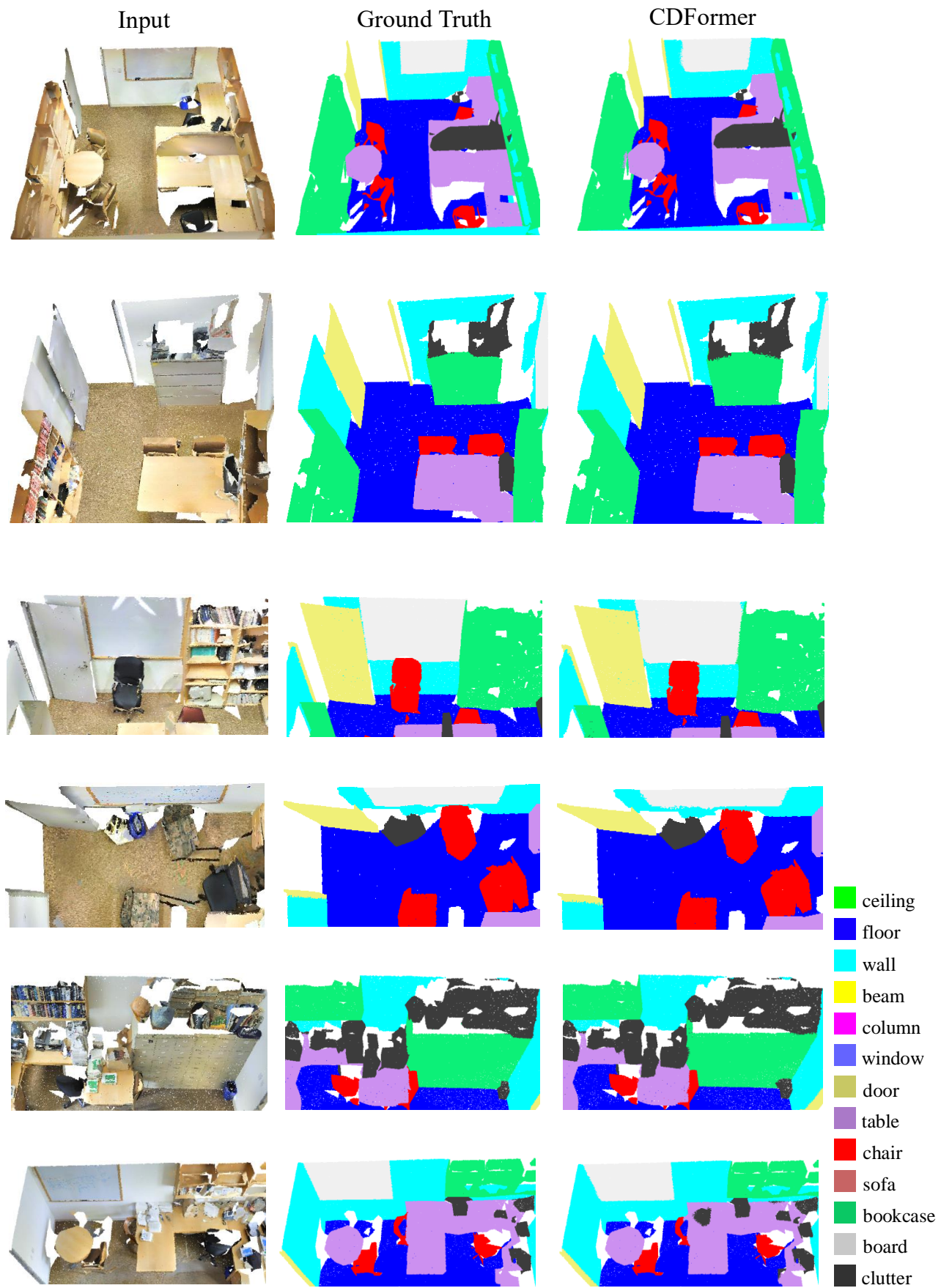


Fig. 6: Visualizations of semantic predictions on Area 5 of S3DIS by comparing CDFormer with the ground truth.

Table 5: Results of the proposed CDFormer and recent state-of-the-arts on Area 5 of S3DIS. The **bold** and underline denote the first and second best performances.

Method	mIoU	mACC	OA	ceiling	floor	wall	beam	column	window	door	table	chair	sofa	bookcase	board	clutter
PointNet (Qi et al., 2017a)	41.1	49.0	-	88.8	97.3	69.8	0.1	3.9	46.3	10.8	59.0	52.6	5.9	40.3	26.4	33.2
SegCloud (Tchapmi et al., 2017)	48.9	57.4	-	90.1	96.1	69.9	0.0	18.4	38.4	23.1	70.4	75.9	40.9	58.4	13.0	41.6
PointCNN (Li et al., 2018b)	57.3	63.9	85.9	92.3	98.2	79.4	0.0	17.6	22.8	62.1	74.4	80.6	31.7	66.7	62.1	56.7
PCT(Guo et al., 2021)	61.3	67.7	-	92.5	98.4	80.6	0.0	19.4	61.6	48.0	76.6	85.2	46.2	67.7	67.9	52.3
HPEIN (Jiang et al., 2019)	61.9	68.3	87.2	91.5	98.2	81.4	0.0	23.3	65.3	40.0	75.5	87.7	58.5	67.8	65.6	49.4
MinkowskiNet (Choy et al., 2019)	65.4	71.7	-	91.8	98.7	86.2	0.0	34.1	48.9	62.4	81.6	89.8	47.2	74.9	74.4	58.6
KPConv (Thomas et al., 2019)	67.1	72.8	-	92.8	97.3	82.4	0.0	23.9	58.0	69.0	81.5	91.0	75.4	75.3	66.7	58.9
CGA-Net(Lu et al., 2021)	68.6	-	-	94.5	98.3	83.0	0.0	25.3	59.6	71.0	92.2	82.6	76.4	77.7	69.5	61.5
CBL (Tang et al., 2022)	69.4	75.2	90.6	93.9	98.4	84.2	0.0	37.0	57.7	71.9	91.7	81.8	77.8	75.6	69.1	62.9
PointFormer (Zhao et al., 2021)	70.4	76.5	90.8	94.0	98.5	86.3	0.0	38.0	63.4	74.3	89.1	82.4	74.3	80.2	76.0	59.3
PointNext-XL (Qian et al., 2022)	70.5	76.8	90.6	94.2	98.5	84.4	0.0	37.7	59.3	74.0	83.1	91.6	77.4	77.2	78.8	60.6
StratifiedFormer (Lai et al., 2022)	<u>72.0</u>	<u>78.1</u>	91.5	96.2	98.7	85.6	0.0	46.1	60.0	76.8	92.6	84.5	77.8	75.2	78.1	64.0
CDFormer	72.2	78.5	<u>91.2</u>	95.1	98.8	86.3	0.0	49.3	62.4	72.1	83.5	92.3	83.9	76.1	75.9	62.7

Table 6: Results of mIoU (%) on both validation and testing set (including per-category IoU) of ScanNetV2.

Method	Val	Test	bathtub	bed	bookshelf	cabinet	chair	counter	curtain	desk	door
PointNet++ (Qi et al., 2017b)	53.5	55.7	73.5	66.1	68.6	49.1	74.4	39.2	53.9	45.1	37.5
RandLA-Net (Hu et al., 2020)	-	64.5	77.8	73.1	69.9	57.7	82.9	44.6	73.6	47.7	52.3
PointConv (Wu et al., 2019)	61.0	66.6	78.1	75.9	69.9	64.4	82.2	47.5	77.9	56.4	50.4
PointASNL (Yan et al., 2020)	63.5	66.6	70.3	78.1	75.1	65.5	83.0	47.1	76.9	47.4	53.7
KPConv (Thomas et al., 2019)	69.2	68.4	84.7	75.8	78.4	64.7	81.4	47.3	77.2	60.5	59.4
CBL (Tang et al., 2022)	-	70.5	76.9	77.5	80.9	68.7	82.0	43.9	81.2	66.1	59.1
PointNext (Qian et al., 2022)	71.5	71.2	-	-	-	-	-	-	-	-	-
PointMeta (Lin et al., 2023)	71.4	83.5	78.5	82.1	68.4	84.6	53.1	86.5	61.4	59.6	-
SparseCNN (Graham et al., 2018)	72.8	72.5	64.7	82.1	84.6	72.1	86.9	53.3	75.4	60.3	61.4
MinkUNet (Choy et al., 2019)	72.2	73.6	85.9	81.8	83.2	70.9	84.0	52.1	85.3	66.0	64.3
StratifiedFormer (Lai et al., 2022)	74.3	74.7	90.1	80.3	84.5	75.7	84.6	51.2	82.5	69.6	64.5
BPNet (Hu et al., 2021)	73.9	74.9	90.9	81.8	81.1	75.2	83.9	48.5	84.2	67.3	64.4
PTv2 (Wu et al., 2022)	75.4	75.2	74.2	80.9	87.2	75.8	86.0	55.2	89.1	61.0	68.7
CDFormer (ours)	76.2	76.6	77.9	79.2	86.1	75.3	88.4	59.1	88.7	62.6	71.3

Method	floor	other.	picture	refrig.	shower.	sink	sofa	table	toilet	wall	window
PointNet++ (Qi et al., 2017b)	94.6	37.6	20.5	40.3	35.6	55.3	64.3	49.7	82.4	75.6	51.5
RandLA-Net (Hu et al., 2020)	94.5	45.4	26.9	48.4	74.9	61.8	73.8	59.9	82.7	79.2	62.1
PointConv (Wu et al., 2019)	95.3	42.8	20.3	58.6	75.4	66.1	75.3	58.8	90.2	81.3	64.2
PointASNL (Yan et al., 2020)	95.1	47.5	27.9	63.5	69.8	67.5	75.1	55.3	81.6	80.6	70.3
KPConv (Thomas et al., 2019)	93.5	45.0	18.1	58.7	80.5	69.0	78.5	61.4	88.2	81.9	63.2
CBL (Tang et al., 2022)	94.5	51.5	17.1	63.3	85.6	72.0	79.6	66.8	88.9	84.7	68.9
PointNext (Qian et al., 2022)	-	-	-	-	-	-	-	-	-	-	-
PointMeta (Lin et al., 2023)	95.3	50.0	24.6	67.4	88.8	69.2	76.4	62.4	84.9	84.4	67.5
SparseCNN (Graham et al., 2018)	95.5	57.2	32.5	71.0	87.0	72.4	82.3	62.8	93.4	86.5	68.3
MinkUNet (Choy et al., 2019)	95.1	54.4	28.6	73.1	89.3	67.5	77.2	68.3	87.4	85.2	72.7
StratifiedFormer (Lai et al., 2022)	95.6	57.6	26.2	74.4	86.1	74.2	77.0	70.5	89.9	86.0	73.4
BPNet (Hu et al., 2021)	95.7	52.8	30.5	77.3	85.9	78.8	81.8	69.3	91.6	85.6	72.3
PTv2 (Wu et al., 2022)	96.0	55.9	30.4	76.6	92.6	76.7	79.7	64.4	94.2	87.6	72.2
CDFormer (ours)	97.6	57.7	33.4	69.8	95.1	82.0	82.8	68.3	95.4	89.3	72.2

Table 7: Ablation study on the CD mechanism.

cfg	LSA	Collect	Distribute	mIoU(%)	mAcc (%)	OA (%)
i	✓			67.6	74.1	89.7
ii	✓	✓		70.1	76.6	90.7
iii	✓		✓	70.3	77.0	90.7
iv	✓	✓	✓	72.2	78.5	91.2

4.5 Ablation Studies

We perform all the ablation studies on Area 5 of S3DIS.

Collect-and-Distribute Mechanism. To explore the effectiveness of the proposed collect-and-distribute (CD) mechanism, we use the counterpart vanilla parameter-free (or tiny) operations as baselines. Specifically, we only keep the max operation to aggregate local features while discarding neighbor self-attention when no *collect*. Also, we adopt an interpolation layer followed by a simple MLP to add back to local points if no *distribute*. In Table 7, we find that without the collect-and-distribute mechanism, it achieves a relatively low mIoU 67.6%, which is then improved by *collect* for catching the long-

Table 8: Ablation study on CAPE.

cfg	QKV	CA	Plain	mIoU (%)	mAcc (%)	OA (%)
i				68.9	76.6	89.7
ii	✓			69.7	76.3	91.0
iii	✓	✓		72.2	78.5	91.2
iv	✓		✓	70.8	77.5	90.9

range dependencies to 70.1%. Furthermore, when further distributing the long-range contexts back to the local points, we achieve the best performances on all metrics, *i.e.*, 72.2% mIoU, 78.5% mAcc, and 91.2% OA. Besides, if without *collect* to explicitly and broadly explore long-range dependencies, using the max aggregation with *Distribute* (see iii) significantly drops the performance from 72.2% to 70.3% on mIoU.

Context-Aware Position Encoding. To evaluate the influence of position encoding, we compare the proposed method with and without using the position encoding in the query, key, and value (**QKV**), respectively. We also compare the context-aware (**CA**) format of position encoding with a vanilla one (*i.e.*, **Plain**) as in Dosovitskiy et al. (2020). As shown in Table 8, without the position encoding, we have dissatisfied results that are consistent with the observations in Lai et al. (2022); Zhao et al. (2021). Next, we employ a normal encoding without context-aware format (see ii) on QKV, *i.e.*, no interaction with the contexts Q, K. This time, it does work but with only marginal improvement. Lastly, when using the proposed CAPE (see iii), it can achieve the state-of-the-art performance 72.2%. Through the dynamic adaptation based on input contexts, the position clues are further enhanced in the proposed CDFormer to effectively learn local-global relations. Additionally, we also show the results of using a vanilla version of position encoding (Dosovitskiy et al., 2020) (see iv) for a fair comparison.

Visualization Comparisons. To further demonstrate the improvement of CDFormer against its baselines, we provide visualizations in Figure 7 by comparing to **w/o CD** (see i in Table 7) and **w/o CAPE** (see ii in Table 8). Taking the first row as an example, without the collect-and-distribute mechanism, the model fails to utilize the semantic-correct long-range contexts and thus can not precisely segment local points; without CAPE, it loses the enhanced position clues for better communication within points and thus obtains dissatisfied results; the CDFormer achieves the convincing predictions as expected.

Model Scalability. We evaluate the model scalability under four stages with [2, 2, 6, 2] blocks via the following three configurations:

Table 9: Ablation study on model scalability.

Model	#Params	mIoU (%)	mAcc (%)	OA (%)
CDFormer-S	3.1M	67.6	74.9	89.8
CDFormer-B	11.7M	69.7	77.1	90.4
CDFormer-L	25.7M	72.2	78.5	91.2

Table 10: Ablation study on number of neighbors.

cfg	K	mIoU (%)	mAcc (%)	OA (%)
i	4	69.2	75.7	90.3
ii	8	71.1	77.9	91.4
iii	16	72.2	78.5	91.2

- CDFormer-S: $\mathcal{C} = [16, 32, 64, 128]$, $\mathcal{H} = [1, 2, 4, 8]$
- CDFormer-B: $\mathcal{C} = [32, 64, 128, 256]$, $\mathcal{H} = [2, 4, 8, 16]$
- CDFormer-L: $\mathcal{C} = [48, 96, 192, 384]$, $\mathcal{H} = [3, 6, 12, 24]$

As shown in Table 9, there are clear performance improvements when using a larger model. For example, the improvements are very impressive in terms of both mIoU and mAcc, *i.e.*, mIoU: 67.6% \rightarrow 69.7% \rightarrow 72.2%; mAcc: 74.9% \rightarrow 77.1% \rightarrow 78.5%. Notably, the consistent improvements by increasing the model size illustrate the extraordinary scalability of the proposed CDFormer for point cloud analysis.

Number of Neighbors. We show the influences for using the different number of neighbors in CD Blocks for patch division, NSA, and NCA. For simplicity, we use the same K for all modules and stages. As shown in Table 10, when increasing the number of neighbors from $K = 4$ to $K = 8$, the improvement (69.2% \rightarrow 71.1%) is significant. This is possibly because a relatively large number of neighbors can bring better long-range contexts, which help the proposed CDFormer learn the local-global structures. Notably, we also find that the advancement from $K = 8$ to $K = 16$ is modest. This kind of saturated phenomenon is expected since too much contexts may introduce different categories of semantics that degrade the local features. Similar observations have also been reported in Zhao et al. (2021). Therefore, we use $K = 16$ as default.

Point Coverage. In Section 3.2, we employ the patch division on the point cloud to generate M patches with K points in each patch. Specifically, we first utilize the FPS (Eldar et al., 1997; Qi et al., 2017b) to downsample the point features $\mathbf{X} \in \mathbb{R}^{N \times C}$ to local patch centers $\hat{\mathbf{X}} \in \mathbb{R}^{M \times C}$ where $M = N/S$ and S is the scale factor. After that, we group the K nearest neighbors around each patch center and reformulate M patches as $\hat{\mathbf{X}} \in \mathbb{R}^{M \times K \times C}$. However, this process may result in some points being left uncovered while others are covered multiple times. Here we present a quantitative analysis. We show the statistics of points covered multi-

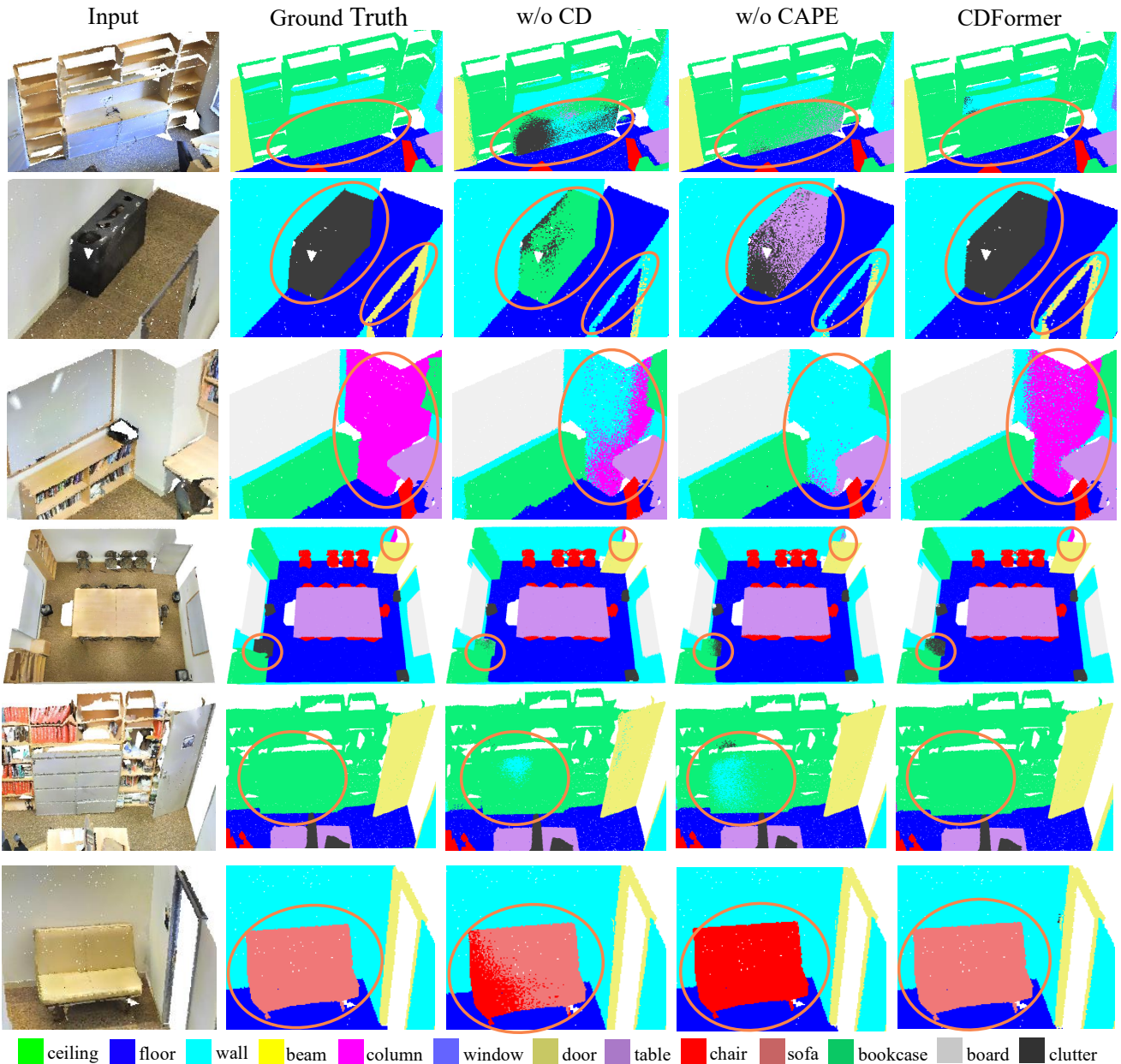


Fig. 7: Visualizations of scene semantic segmentation on Area 5 of S3DIS by comparing CDFormer with its baselines and ground truth. The improved areas against baselines are highlighted by the orange circles.

ple times or uncovered at different stages of CDFormer on the S3DIS dataset in Table 11. As we can see, no more than 0.4% of all points are uncovered across all stages. In addition, each point is covered by two times on average due to $M = N/8$ and $MK = 2N$, and maximally covered by six times. As a result, their impact should be negligible.

Activation Maps. We illustrate the activation maps of different stages of CDFormer to show the effectiveness of collect-and-distribute mechanism in Figure 8. Specifically, we backtrack the feature of interest from

Table 11: Statistics of point coverage on different stages.

Stage	Uncovered Ratio	Maximum Times Covered
1	0.28%	6.00
2	0.28%	5.26
3	0.38%	4.62
4	0.24%	4.18

each stage and calculate the gradients for each input point. A larger gradient indicates that the current point contributes more to the feature of interest. In rows one

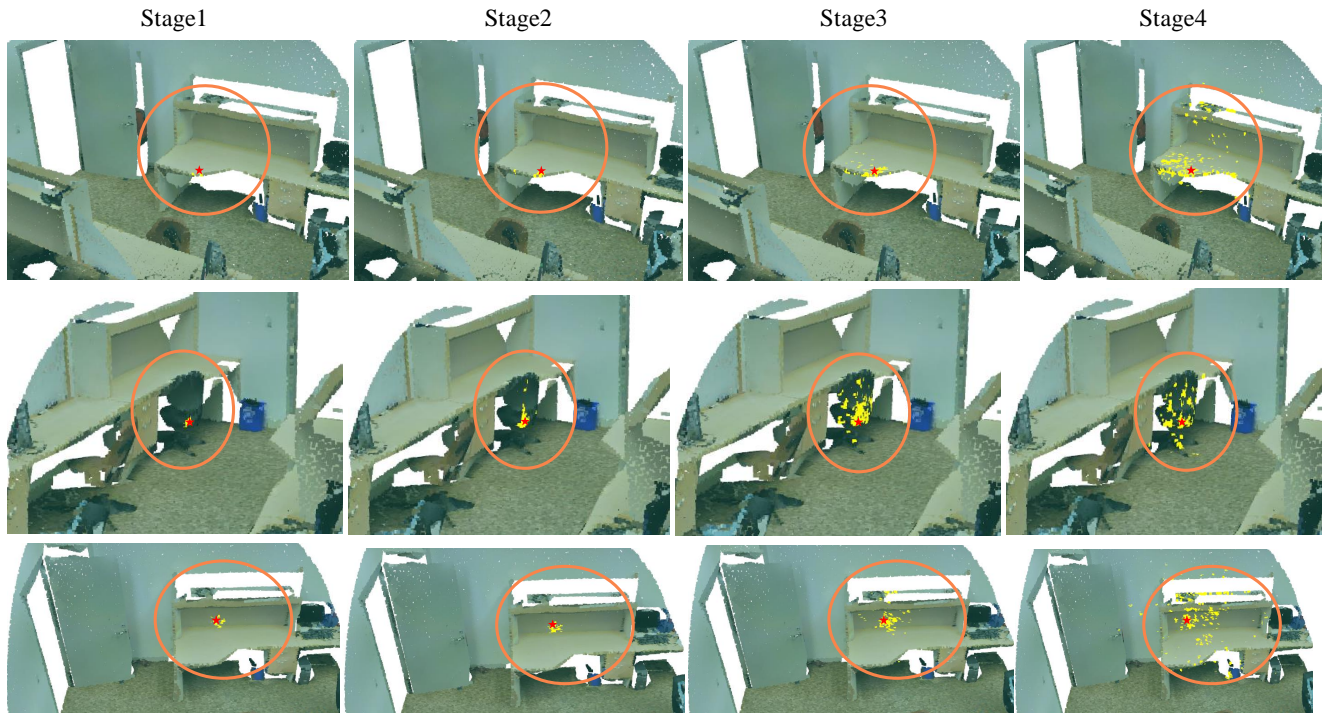


Fig. 8: Visualization of activation maps where region of interest are highlighted by orange circles at different stages of CDFormer given the feature of interest (marked as red star).

to three, we select points of interest from classes “table”, “chair”, and “bookcase” respectively. As observed, the number of perceptive points increases inside the same category as the stage progresses due to the collect-and-distribute mechanism. For example, in the case of a point on the edge of a table, it can first interact with more points along that edge before reaching points inside the table itself. Similarly, for a point on a chair, it gradually captures all relevant points distributed across its surface while avoiding irrelevant or nearby points from other categories.

5 Conclusion

In this paper, we introduce the innovative CDFormer for 3D point cloud analysis. With our proposed collect-and-distribute mechanism, it can capture both short-and long-range contexts simultaneously, effectively learning local-global representations of point clouds. Furthermore, we enhance position clues dynamically via context-aware position encoding to facilitate communication among point features. We conducted comprehensive experiments on S3DIS, ScanNetV2, ShapeNetPart, ModelNet40, and ScanObjectNN for segmentation and classification tasks to demonstrate the superiority of CDFormer and the advantages of each design choice.

References

- Abadi M, Barham P, Chen J, Chen Z, Davis A, Dean J, Devin M, Ghemawat S, Irving G, Isard M, Kudlur M, Levenberg J, Monga R, Moore S, Murray DG, Steiner B, Tucker P, Vasudevan V, Warden P,wicke M, Yu Y, Zheng X (2016) Tensorflow: A system for large-scale machine learning. In: 12th USENIX Symposium on Operating Systems Design and Implementation (OSDI 16), pp 265–283, URL <https://www.usenix.org/system/files/conference/osdi16/osdi16-abadi.pdf> 2
- Aksoy EE, Baci S, Cavdar S (2020) Salsanet: Fast road and vehicle segmentation in lidar point clouds for autonomous driving. In: IEEE Intelligent Vehicles Symposium, pp 926–932 1
- Armeni I, Sener O, Zamir AR, Jiang H, Brilakis I, Fischer M, Savarese S (2016) 3d semantic parsing of large-scale indoor spaces. In: IEEE/CVF Conference on Computer Vision and Pattern Recognition (CVPR), pp 1534–1543 2, 3, 6, 7
- Brown T, Mann B, Ryder N, Subbiah M, Kaplan JD, Dhariwal P, Neelakantan A, Shyam P, Sastry G, Askell A, et al. (2020) Language models are few-shot learners. Advances in Neural Information Processing Systems (NeurIPS) 33:1877–1901 1

- Cheng R, Razani R, Taghavi E, Li E, Liu B (2021a) 2-s3net: Attentive feature fusion with adaptive feature selection for sparse semantic segmentation network. In: IEEE/CVF Conference on Computer Vision and Pattern Recognition (CVPR), pp 12547–12556 [3](#)
- Cheng S, Chen X, He X, Liu Z, Bai X (2021b) Pra-net: Point relation-aware network for 3d point cloud analysis. *IEEE Transactions on Image Processing (TIP)* 30:4436–4448 [7](#)
- Choy C, Gwak J, Savarese S (2019) 4d spatio-temporal convnets: Minkowski convolutional neural networks. In: IEEE/CVF Conference on Computer Vision and Pattern Recognition (CVPR), pp 3075–3084 [10](#)
- Chu X, Tian Z, Wang Y, Zhang B, Ren H, Wei X, Xia H, Shen C (2021) Twins: Revisiting the design of spatial attention in vision transformers. *Advances in Neural Information Processing Systems (NeurIPS)* 34 [2](#)
- Cortinhal T, Tzelepis G, Aksoy EE (2020) Salsanext: Fast, uncertainty-aware semantic segmentation of lidar point clouds. In: International Symposium on Visual Computing (ISVC), pp 207–222 [3](#)
- Dai A, Chang AX, Savva M, Halber M, Funkhouser T, Nießner M (2017) Scannet: Richly-annotated 3d reconstructions of indoor scenes. In: IEEE/CVF Conference on Computer Vision and Pattern Recognition (CVPR), pp 5828–5839 [2](#), [6](#), [8](#)
- Devlin J, Chang MW, Lee K, Toutanova K (2018) Bert: Pre-training of deep bidirectional transformers for language understanding. *arXiv preprint arXiv:1810.04805* [1](#), [2](#)
- Dosovitskiy A, Beyer L, Kolesnikov A, Weissenborn D, Zhai X, Unterthiner T, Dehghani M, Minderer M, Heigold G, Gelly S, et al. (2020) An image is worth 16x16 words: Transformers for image recognition at scale. *arXiv preprint arXiv:2010.11929* [1](#), [2](#), [3](#), [5](#), [11](#)
- Eldar Y, Lindenbaum M, Porat M, Zeevi YY (1997) The farthest point strategy for progressive image sampling. *IEEE Transactions on Image Processing (TIP)* 6(9):1305–1315 [4](#), [11](#)
- Fan H, Xiong B, Mangalam K, Li Y, Yan Z, Malik J, Feichtenhofer C (2021a) Multiscale vision transformers. In: IEEE/CVF International Conference on Computer Vision (ICCV), pp 6824–6835 [2](#)
- Fan S, Dong Q, Zhu F, Lv Y, Ye P, Wang FY (2021b) Scf-net: Learning spatial contextual features for large-scale point cloud segmentation. In: Proceedings of the IEEE/CVF Conference on Computer Vision and Pattern Recognition, pp 14504–14513 [8](#)
- Goyal A, Law H, Liu B, Newell A, Deng J (2021) Revisiting point cloud shape classification with a simple and effective baseline. In: International Conference on Machine Learning (ICML), PMLR, pp 3809–3820 [7](#)
- Graham B, Engelcke M, Van Der Maaten L (2018) 3d semantic segmentation with submanifold sparse convolutional networks. In: IEEE/CVF Conference on Computer Vision and Pattern Recognition (CVPR), pp 9224–9232 [10](#)
- Gu J, Kwon H, Wang D, Ye W, Li M, Chen YH, Lai L, Chandra V, Pan DZ (2022) Multi-scale high-resolution vision transformer for semantic segmentation. In: IEEE/CVF Conference on Computer Vision and Pattern Recognition (CVPR), pp 12094–12103 [2](#)
- Guo MH, Cai JX, Liu ZN, Mu TJ, Martin RR, Hu SM (2021) Pct: Point cloud transformer. *Computational Visual Media* 7(2):187–199 [1](#), [3](#), [7](#), [10](#)
- Hamdi A, Giancola S, Ghanem B (2021) Mvtn: Multi-view transformation network for 3d shape recognition. In: IEEE/CVF International Conference on Computer Vision (ICCV), pp 1–11 [7](#)
- Han L, Zheng T, Xu L, Fang L (2020) Occuseg: Occupancy-aware 3d instance segmentation. In: IEEE/CVF Conference on Computer Vision and Pattern Recognition (CVPR), pp 2940–2949 [8](#)
- Hu Q, Yang B, Xie L, Rosa S, Guo Y, Wang Z, Trigoni N, Markham A (2020) Randla-net: Efficient semantic segmentation of large-scale point clouds. In: IEEE/CVF Conference on Computer Vision and Pattern Recognition (CVPR), pp 11108–11117 [8](#), [10](#)
- Hu W, Zhao H, Jiang L, Jia J, Wong TT (2021) Bidirectional projection network for cross dimension scene understanding. In: IEEE/CVF Conference on Computer Vision and Pattern Recognition (CVPR), pp 14373–14382 [10](#)
- Huang Q, Wang W, Neumann U (2018) Recurrent slice networks for 3d segmentation of point clouds. In: IEEE/CVF Conference on Computer Vision and Pattern Recognition (CVPR), pp 2626–2635 [8](#)
- Jiang L, Zhao H, Liu S, Shen X, Fu CW, Jia J (2019) Hierarchical point-edge interaction network for point cloud semantic segmentation. In: IEEE/CVF International Conference on Computer Vision (ICCV), pp 10433–10441 [10](#)
- Komarichev A, Zhong Z, Hua J (2019) A-cnn: Annularly convolutional neural networks on point clouds. In: IEEE/CVF Conference on Computer Vision and Pattern Recognition (CVPR), pp 7421–7430 [7](#)
- Lai X, Liu J, Jiang L, Wang L, Zhao H, Liu S, Qi X, Jia J (2022) Stratified transformer for 3d point cloud segmentation. *IEEE/CVF Conference on Computer Vision and Pattern Recognition (CVPR)* [1](#), [2](#), [3](#), [5](#), [6](#), [7](#), [10](#), [11](#)
- Li J, Chen BM, Lee GH (2018a) So-net: Self-organizing network for point cloud analysis. In: IEEE/CVF Conference on Computer Vision and Pattern Recognition

- (CVPR), pp 9397–9406 **7**
- Li W, Wang X, Xia X, Wu J, Xiao X, Zheng M, Wen S (2022a) Sepvit: Separable vision transformer. arXiv preprint arXiv:220315380 **2**
- Li X, Du S, Li G, Li H (2019) Integrate point-cloud segmentation with 3d lidar scan-matching for mobile robot localization and mapping. *Sensors* 20(1):237 **1**
- Li Y, Bu R, Sun M, Wu W, Di X, Chen B (2018b) Pointcnn: Convolution on x-transformed points. *Advances in Neural Information Processing Systems (NeurIPS)* 31 **1, 3, 7, 8, 10**
- Li Y, Ma L, Zhong Z, Liu F, Chapman MA, Cao D, Li J (2020) Deep learning for lidar point clouds in autonomous driving: A review. *IEEE Transactions on Neural Networks and Learning Systems (TNNLS)* 32(8):3412–3432 **1**
- Li Y, Wu CY, Fan H, Mangalam K, Xiong B, Malik J, Feichtenhofer C (2022b) Mvitv2: Improved multiscale vision transformers for classification and detection. In: *IEEE/CVF Conference on Computer Vision and Pattern Recognition (CVPR)* **2**
- Lin H, Zheng X, Li L, Chao F, Wang S, Wang Y, Tian Y, Ji R (2023) Meta architecture for point cloud analysis. *IEEE/CVF Conference on Computer Vision and Pattern Recognition (CVPR)* **10**
- Liu Z, Hu H, Cao Y, Zhang Z, Tong X (2020) A closer look at local aggregation operators in point cloud analysis. In: *European Conference on Computer Vision (ECCV)*, Springer, pp 326–342 **7**
- Liu Z, Lin Y, Cao Y, Hu H, Wei Y, Zhang Z, Lin S, Guo B (2021a) Swin transformer: Hierarchical vision transformer using shifted windows. In: *IEEE/CVF International Conference on Computer Vision (ICCV)*, pp 10012–10022 **1, 2, 3**
- Liu Z, Qi X, Fu CW (2021b) One thing one click: A self-training approach for weakly supervised 3d semantic segmentation. In: *IEEE/CVF Conference on Computer Vision and Pattern Recognition (CVPR)*, pp 1726–1736 **8**
- Loshchilov I, Hutter F (2017) Decoupled weight decay regularization. arXiv preprint arXiv:171105101 **6**
- Lu T, Wang L, Wu G (2021) Cga-net: Category guided aggregation for point cloud semantic segmentation. In: *Proceedings of the IEEE/CVF Conference on Computer Vision and Pattern Recognition*, pp 11693–11702 **10**
- Ma X, Qin C, You H, Ran H, Fu Y (2022) Rethinking network design and local geometry in point cloud: A simple residual mlp framework. *International Conference on Learning Representations (ICLR)* **1, 3, 7**
- Milioto A, Vizzo I, Behley J, Stachniss C (2019) Rangenet++: Fast and accurate lidar semantic segmentation. In: *IEEE/RSJ International Conference on Intelligent Robots and Systems (IROS)*, pp 4213–4220 **3**
- Pang Y, Wang W, Tay FE, Liu W, Tian Y, Yuan L (2022) Masked autoencoders for point cloud self-supervised learning. arXiv preprint arXiv:220306604 **3**
- Park C, Jeong Y, Cho M, Park J (2022) Fast point transformer. *IEEE/CVF Conference on Computer Vision and Pattern Recognition (CVPR)* **1, 3**
- Paszke A, Gross S, Massa F, Lerer A, Bradbury J, Chanan G, Killeen T, Lin Z, Gimelshein N, Antiga L, et al. (2019) Pytorch: An imperative style, high-performance deep learning library. *Advances in Neural Information Processing Systems (NeurIPS)* 32 **2**
- Qi CR, Su H, Mo K, Guibas LJ (2017a) Pointnet: Deep learning on point sets for 3d classification and segmentation. In: *IEEE/CVF Conference on Computer Vision and Pattern Recognition (CVPR)*, pp 652–660 **1, 3, 7, 8, 10**
- Qi CR, Yi L, Su H, Guibas LJ (2017b) Pointnet++: Deep hierarchical feature learning on point sets in a metric space. *Advances in Neural Information Processing Systems (NeurIPS)* 30 **1, 3, 4, 7, 8, 10, 11**
- Qian G, Hammoud H, Li G, Thabet A, Ghanem B (2021) Assanet: An anisotropic separable set abstraction for efficient point cloud representation learning. *Advances in Neural Information Processing Systems (NeurIPS)* 34:28119–28130 **7**
- Qian G, Li Y, Peng H, Mai J, Hammoud HAAK, Elhoseiny M, Ghanem B (2022) Pointnext: Revisiting pointnet++ with improved training and scaling strategies. *Advances in Neural Information Processing Systems (NeurIPS)* **3, 6, 7, 8, 10**
- Qiu H, Yu B, Tao D (2022) GFNet: Geometric flow network for 3d point cloud semantic segmentation. *Transactions on Machine Learning Research* URL <https://openreview.net/forum?id=LSAAL57Yts> **3**
- Qiu H, Yu B, Chen Y, Tao D (2023) Pointhr: Exploring high-resolution architectures for 3d point cloud segmentation. arXiv preprint arXiv:231007743 **3**
- Qiu S, Anwar S, Barnes N (2021a) Dense-resolution network for point cloud classification and segmentation. In: *IEEE/CVF Winter Conference on Applications of Computer Vision (WACV)*, pp 3813–3822 **7**
- Qiu S, Anwar S, Barnes N (2021b) Geometric back-projection network for point cloud classification. *IEEE Transactions on Multimedia* 24:1943–1955 **7**
- Qiu S, Anwar S, Barnes N (2021c) Semantic segmentation for real point cloud scenes via bilateral augmentation and adaptive fusion. In: *IEEE/CVF Conference on Computer Vision and Pattern Recognition (CVPR)*, pp 1757–1767 **8**

- Robert D, Vallet B, Landrieu L (2022) Learning multi-view aggregation in the wild for large-scale 3d semantic segmentation. In: IEEE/CVF Conference on Computer Vision and Pattern Recognition (CVPR), pp 5575–5584 [8](#)
- Smith LN, Topin N (2019) Super-convergence: Very fast training of neural networks using large learning rates. In: Artificial intelligence and machine learning for multi-domain operations applications, SPIE, vol 11006, pp 369–386 [6](#)
- Tang H, Liu Z, Zhao S, Lin Y, Lin J, Wang H, Han S (2020) Searching efficient 3d architectures with sparse point-voxel convolution. In: European Conference on Computer Vision (ECCV), pp 685–702 [3](#)
- Tang L, Zhan Y, Chen Z, Yu B, Tao D (2022) Contrastive boundary learning for point cloud segmentation. In: IEEE/CVF Conference on Computer Vision and Pattern Recognition (CVPR), pp 8489–8499 [8](#), [10](#)
- Tang L, Chen Z, Zhao S, Wang C, Tao D (2023) All points matter: Entropy-regularized distribution alignment for weakly-supervised 3d segmentation. In: Advances in Neural Information Processing Systems (NeurIPS), URL <https://openreview.net/forum?id=utQms7PPx5> [3](#)
- Tchapmi L, Choy C, Armeni I, Gwak J, Savarese S (2017) Segcloud: Semantic segmentation of 3d point clouds. In: International Conference on 3D Vision (3DV), IEEE, pp 537–547 [10](#)
- Thomas H, Qi CR, Deschaud JE, Marcotegui B, Goulette F, Guibas LJ (2019) Kpconv: Flexible and deformable convolution for point clouds. In: IEEE/CVF International Conference on Computer Vision (ICCV), pp 6411–6420 [1](#), [3](#), [7](#), [8](#), [10](#)
- Uy MA, Pham QH, Hua BS, Nguyen T, Yeung SK (2019) Revisiting point cloud classification: A new benchmark dataset and classification model on real-world data. In: IEEE/CVF International Conference on Computer Vision (ICCV), pp 1588–1597 [2](#), [6](#), [7](#)
- Vaswani A, Shazeer N, Parmar N, Uszkoreit J, Jones L, Gomez AN, Kaiser L, Polosukhin I (2017) Attention is all you need. Advances in Neural Information Processing Systems (NeurIPS) 30 [1](#), [2](#), [5](#)
- Wang W, Xie E, Li X, Fan DP, Song K, Liang D, Lu T, Luo P, Shao L (2021) Pyramid vision transformer: A versatile backbone for dense prediction without convolutions. In: IEEE/CVF International Conference on Computer Vision (ICCV), pp 568–578 [1](#), [2](#)
- Wang W, Xie E, Li X, Fan DP, Song K, Liang D, Lu T, Luo P, Shao L (2022) Pvt v2: Improved baselines with pyramid vision transformer. Computational Visual Media 8(3):415–424 [1](#), [2](#)
- Wang Y, Sun Y, Liu Z, Sarma SE, Bronstein MM, Solomon JM (2019) Dynamic graph cnn for learning on point clouds. ACM Transactions On Graphics (TOG) 38(5):1–12 [1](#), [3](#), [7](#)
- Wu K, Peng H, Chen M, Fu J, Chao H (2021) Rethinking and improving relative position encoding for vision transformer. In: IEEE/CVF International Conference on Computer Vision (ICCV), pp 10033–10041 [5](#)
- Wu W, Qi Z, Fuxin L (2019) Pointconv: Deep convolutional networks on 3d point clouds. In: IEEE/CVF Conference on Computer Vision and Pattern Recognition (CVPR), pp 9621–9630 [7](#), [10](#)
- Wu X, Lao Y, Jiang L, Liu X, Zhao H (2022) Point transformer v2: Grouped vector attention and partition-based pooling. In: Advances in Neural Information Processing Systems (NeurIPS) [6](#), [8](#), [10](#)
- Wu Z, Song S, Khosla A, Yu F, Zhang L, Tang X, Xiao J (2015) 3d shapenets: A deep representation for volumetric shapes. In: IEEE/CVF Conference on Computer Vision and Pattern Recognition (CVPR), pp 1912–1920 [2](#), [6](#)
- Xiang T, Zhang C, Song Y, Yu J, Cai W (2021) Walk in the cloud: Learning curves for point clouds shape analysis. In: IEEE/CVF International Conference on Computer Vision (ICCV), pp 915–924 [7](#)
- Xu C, Zhai B, Wu B, Li T, Zhan W, Vajda P, Keutzer K, Tomizuka M (2021a) You only group once: Efficient point-cloud processing with token representation and relation inference module. In: IEEE/RSJ International Conference on Intelligent Robots and Systems (IROS), IEEE, pp 4589–4596 [3](#)
- Xu M, Ding R, Zhao H, Qi X (2021b) Paconv: Position adaptive convolution with dynamic kernel assembling on point clouds. In: IEEE/CVF Conference on Computer Vision and Pattern Recognition (CVPR), pp 3173–3182 [7](#)
- Xu Y, Fan T, Xu M, Zeng L, Qiao Y (2018) Spidercnn: Deep learning on point sets with parameterized convolutional filters. In: European Conference on Computer Vision (ECCV), pp 87–102 [7](#)
- Yan X, Zheng C, Li Z, Wang S, Cui S (2020) Pointasnl: Robust point clouds processing using nonlocal neural networks with adaptive sampling. In: IEEE/CVF Conference on Computer Vision and Pattern Recognition (CVPR), pp 5589–5598 [7](#), [10](#)
- Yang J, Li C, Zhang P, Dai X, Xiao B, Yuan L, Gao J (2021) Focal self-attention for local-global interactions in vision transformers. Advances in Neural Information Processing Systems (NeurIPS) [2](#)
- Yang L, Liu Y, Peng J, Liang Z (2020) A novel system for off-line 3d seam extraction and path planning based on point cloud segmentation for arc welding

- robot. *Robotics and Computer-Integrated Manufacturing* 64:101929 [1](#)
- Yang YQ, Guo YX, Xiong JY, Liu Y, Pan H, Wang PS, Tong X, Guo B (2023) Swin3d: A pretrained transformer backbone for 3d indoor scene understanding. arXiv preprint arXiv:230406906 [8](#)
- Yi L, Kim VG, Ceylan D, Shen IC, Yan M, Su H, Lu C, Huang Q, Sheffer A, Guibas L (2016) A scalable active framework for region annotation in 3d shape collections. *SIGGRAPH Asia* [2](#), [6](#), [7](#)
- Yu X, Tang L, Rao Y, Huang T, Zhou J, Lu J (2022) Point-bert: Pre-training 3d point cloud transformers with masked point modeling. *IEEE/CVF Conference on Computer Vision and Pattern Recognition (CVPR)* [3](#)
- Zhang J, Chen L, Ouyang B, Liu B, Zhu J, Chen Y, Meng Y, Wu D (2022) Pointcutmix: Regularization strategy for point cloud classification. *Neurocomputing* 505:58–67 [6](#)
- Zhang Y, Zhou Z, David P, Yue X, Xi Z, Gong B, Foroosh H (2020) Polarnet: An improved grid representation for online lidar point clouds semantic segmentation. In: *IEEE/CVF Conference on Computer Vision and Pattern Recognition (CVPR)*, pp 9601–9610 [3](#)
- Zhang Z, Hua BS, Yeung SK (2019) Shellnet: Efficient point cloud convolutional neural networks using concentric shells statistics. *IEEE/CVF International Conference on Computer Vision (ICCV)* pp 1607–1616 [8](#)
- Zhao H, Jiang L, Fu CW, Jia J (2019) Pointweb: Enhancing local neighborhood features for point cloud processing. In: *IEEE/CVF Conference on Computer Vision and Pattern Recognition (CVPR)*, pp 5565–5573 [8](#)
- Zhao H, Jiang L, Jia J, Torr PH, Koltun V (2021) Point transformer. In: *IEEE/CVF International Conference on Computer Vision (ICCV)*, pp 16259–16268 [1](#), [2](#), [3](#), [5](#), [6](#), [7](#), [8](#), [10](#), [11](#)
- Zhu X, Zhou H, Wang T, Hong F, Ma Y, Li W, Li H, Lin D (2021) Cylindrical and asymmetrical 3d convolution networks for lidar segmentation. In: *IEEE/CVF Conference on Computer Vision and Pattern Recognition (CVPR)*, pp 9939–9948 [3](#)